IET Optoelectronics

Selected Papers from Semiconductor and Integrated Optoelectronics (SIOE) 2018

IET Journals
The Institution of Engineering and Technology

Restraining effect of film thickness on the behaviour of amplified spontaneous emission from methylammonium lead iodide perovskite

ISSN 1751-8768
Received on 8th May 2018
Revised 19th July 2018
Accepted on 31st July 2018
E-First on 5th September 2018
doi: 10.1049/iet-opt.2018.5035
www.ietdl.org

Saif M.H. Qaid[1,2] ✉, M. Naziruddin Khan[3], Abdulaziz Alqasem[1], Mahmoud Hezam[3], Abdullah Aldwayyan[1,3]

[1]*Physics and Astronomy Department, Photonics Lab, King Saud University, Riyadh, Saudi Arabia*
[2]*Department of Physics, Faculty of Science, Ibb University, Ibb, Yemen*
[3]*King Abdullah Institute for Nanotechnology, King Saud University, Riyadh, Saudi Arabia*
✉ *E-mail: saif.m.h.qaid@gmail.com*

Abstract: The authors report amplified spontaneous emission (ASE) behaviour from methylammonium lead iodide ($CH_3NH_3PbI_3$) perovskite films of different thicknesses. The ASE threshold carrier density noticeably decreased with thickness, indicating the existence of different traps with perovskite films of smaller thicknesses. We attribute this behaviour to the presence of surface states, whose origin can result from different practical fabrication steps with samples of small thicknesses. The ASE threshold carrier density increased from 3.29×10^{18} cm^{-3} at a film thickness of 650 nm to 7.73×10^{18} cm^{-3} at a film thickness of 80 nm. This work warns that while decreasing the film thickness is of practical importance to reduce the ASE threshold pump current, e.g. in electrically driven light-emitting diodes, the solution processing of perovskites, newly re-discovered for their potential photonic and photovoltaic applications, can be a restraining factor. Band gap renormalisation (BGR) is also observed in the prepared films as a redshift in the ASE peak with increasing the pump power, and the BGR coefficient is estimated to be $\sim 6.3 \times 10^{-8}$ eV cm.

1 Introduction

In recent years, organometal halide perovskites have gained a tremendous research boost as efficient photovoltaic light harvesters and as promising photonic materials as well. The physical properties of $MAPbX_3$ thin films have further been cemented toward light-emitting diodes [1–3]. These materials have the crystalline structure ABX_3, where A is an organic molecule such as methylammonium (MA) or formamidinium, B is an inorganic metal (e.g. Pb and Sn), and X is a halogen atom (Cl, Br, and I).

For photonic applications, the easily tunable direct bandgap of this class of materials and the low-cost solution-based fabrication process have been important triggers for extensive research efforts to be instigated [4–6]. As an evidence for stimulated emission, and thus promise for lasing applications across the visible and near-infrared [5, 7, 8], amplified spontaneous emission (ASE) using optical pumping has been well demonstrated for different OMHP systems with low ASE threshold pump energies [5, 9]. An indication of low threshold ASE from $CH_3NH_3PbI_3$ thin films and vertical microcavity lasing from $CH_3NH_3PbI_3$ crystals was first reported early in 2014 [10, 11]. The quality of the perovskite material can be altered by tuning the different cations and anions in the perovskite lattice [10]. Since then, such hybrid perovskite materials have shown great capacity for light-emissive technologies due to their spectral tunability and high photoluminescence (PL) yield. $MAPbX_3$ films were found to exhibit random lasing [12] as well as lasing from different geometrically designed resonators [13–15]. Optical gain from perovskite nanostructures [14, 16] and colloidal perovskite nanocrystals [17–19] have also been demonstrated.

For electrically driven lasing devices, reducing the thickness of the optically active layer is an essential engineering step to reduce the ASE threshold pump current. Therefore, careful investigation of the effect of perovskite thickness is an important prerequisite, especially with the chemical nature of perovskite film deposition.

In this work, we report a careful study on the effect of thickness on the ASE threshold pump energy, where the renowned MA lead iodide perovskite ($CH_3NH_3PbI_3$) has been chosen for this purpose. Briefly, the results show that the ASE threshold pump energy increases from 2.35 to 3.65 μJ/cm^2 when the thickness is increased from 80 to 650 nm. However, careful calculation of the ASE threshold carrier density (n_{th}) with the different thicknesses revealed an unexpected dependence, where n_{th} noticeably decreases with thickness. The value of n_{th} decreased from 7.73×10^{18} to 3.29×10^{18} cm^{-3} when the film thickness is increased from 80 to 650 nm. Bandgap renormalisation (BGR) was also studied in our work and observed as a systematic red shift of the ASE emission with increasing pump energy. A BGR constant of 6.3×10^{-8} eV cm was obtained.

2 Experimental

All samples were fabricated on microscopic glass slide substrates by the spin-coating technique. First, glass substrates were sequentially cleaned in detergent water, deionised water, and ethanol (for 15 min each) by an ultrasonic bath. The single-step spin-coating deposition approach is adopted to prepare the films [20–24]. In this method, the deposition solution consists of MA iodide (CH_3NH_3I) and lead iodide (PbI_2) precursors dissolved in a mixed solvent of dimethyl formamide:dimethyl sulphoxide having a 1:1 volume ratio. The total weight of the two dissolved precursors, i.e. CH_3NH_3I (Sigma Aldrich) and PbI_2 (Sigma Aldrich), was used as a tuning factor for the resulting film thickness [4]. Therefore, the mixture of the two precursors was dissolved in different weight concentrations of 10, 20, 30 and 40%. Each weight concentration produced a different film thickness. Weight concentrations of 10, 20, 30 and 40%, respectively, produced film thicknesses of 80, 230, 500 and 650 nm. After that, the coated films were placed on a hotplate set at 100°C for 30 min in ambient air.

The film thickness was measured using a surface porfilometer (Veeco Dektak 150). The absorption measurements were carried out using a Jasco V-650 spectrophotometer. The films were excited with 70 ps laser pulses of variable power having an excitation

© The Institution of Engineering and Technology 2018

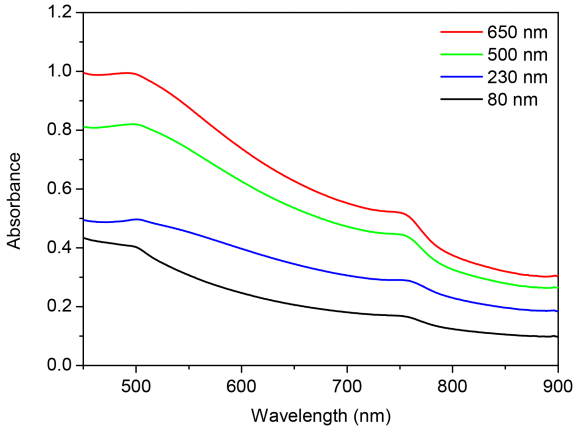

Fig. 1 *Absorption spectra of $MAPbI_3$ perovskite films of different thicknesses*

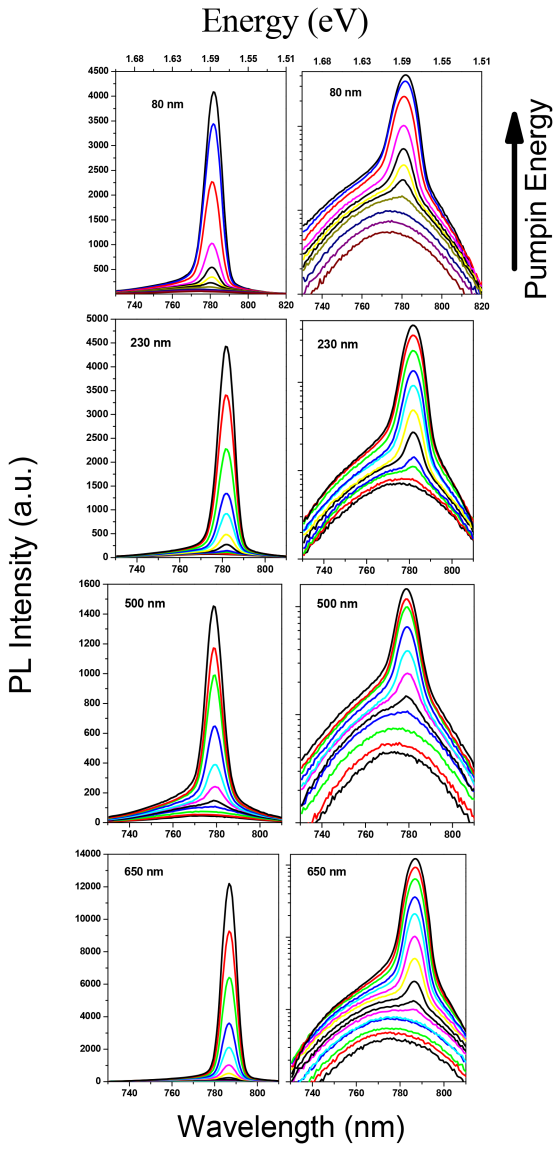

Fig. 2 *PL spectra evolution with increasing excitation pump energy for $MAPbI_3$ perovskite films of different thicknesses*

wavelength of 532 nm and a repetition rate of 15 Hz. The laser pulse source is a Q-switched Nd:YAG Pico Second Tunable Laser System (LS-2151, LOTTIS II). The beam size was focused to ~ 2 mm by a convenient lens. The energy of the pulses was controlled using neutral density filters. The output signal from the sample was collected through an optical fibre with a collimating lens attached with a spectrograph (QE65 Pro, Ocean Optics). The excited carrier density in the films (n_{th}) was estimated using the linear absorbance spectra of the films, their measured thicknesses and energies of the incident laser pulses.

3 Results

3.1 Linear absorption and power-dependent PL properties

Fig. 1 shows the linear absorption spectra of the four prepared films. The absorption onset can be observed at ~780 nm for all samples, which corresponds to the near band edge of $MAPbI_3$ [4, 25, 26]. No shifts in fundamental absorption peaks of the perovskite $MAPbI_3$ are noticed for all the thin films under study. The absorbance increases with film thickness, as predictable, for which the absorption coefficient can be estimated to be in the range of ~10^4 cm^{-1} in the visible range for all the prepared films, which is in agreement with countless reports in the literature [4, 25, 26].

We then study the influence of thickness variation of the emission characteristics of $MAPbI_3$ films with photo-excitation power. All films of thicknesses 80, 230, 500 and 650 nm were systematically studied and pumped with increasing excitation energy. We found for all prepared films of different thicknesses, the PL emission has an abrupt increase after a certain pump power threshold, indicating ASE. The spectral ASE behaviours from the four perovskite films are shown in Fig. 2, which presents spectral PL, for each film, at various pumping energies. The right column shows the PL intensity on the log scale for clarity of the ASE onset. One can notice the transition from spontaneous emission (SE) to ASE regimes by looking at the linewidth narrowing, which decreases from a broad peak of ~50–60 nm linewidth below the ASE threshold to a sharp peak of ~6–8 nm linewidth above the threshold. This linewidth narrowing is a clear signature of optical gain (or ASE) [10, 11, 27–29]. The samples were excited up to 5 times the threshold energy and showed stable narrowing of the full-width-at-half-maximum values at around ~7 nm for all tested thicknesses. The 650 nm film has a relativity narrower ASE peak. Additionally, in addition to the broad PL peak, a new PL peak emerges at the low energy side upon the onset of ASE, which we call the ASE peak. The origin of this splitting of the broad emission band above the threshold is debatable in the literature [10, 30].

Above the ASE threshold, the ASE peak is red-shifted upon further increasing the excitation energy. Over an excitation energy range between 2 and 10 μJ, an ASE redshift of up to ~ 10 nm is observed, which is consistent with previous reports [10, 27–29]. Fig. 3 shows the ASE peak position dependence on excitation energy. Although the trend is similar, the sensitivity of the ASE peak position to the excitation energy is, in general, larger for thicker films. For example, a redshift of 11 nm can be obtained for the 650 nm film compared to 7 nm for the 230 nm film under 3 μJ variation in excitation energy. In fact, ASE originally developed due to an increase in both the optical gain and absorption rate. The balance between optical gain and self-absorption gives rise to a red-shifted ASE peak that is located near the tail of the absorption edge [10].

Fig. 4 shows the integrated PL versus incident energy density for the prepared films. The integrated PL is extracted by convenient Gaussian peak fitting of the PL emission curves of Fig. 2. For each sample, we can define two regions: namely spontaneous (below threshold) and stimulated (above threshold) emission. Besides the linewidth narrowing discussed above, the existence of the two regions of emission is considered a strong indication of coherent beam regime [10]. The threshold energy can be estimated as the intersection point between the SE and the ASE lines. ASE threshold energies were found to be 2.35, 2.91, 3.65 and 3.78 μJ/cm^2, respectively, for the 80, 230, 500 and 650 nm films. These low ASE threshold values are characteristic of perovskite materials and are attributable to their small capture cross-sections of trap states, low bimolecular recombination and ‘slow’ Auger recombination properties [10, 14]. The slope of the PL versus energy density curves in the ASE region is an indicator of the quantum efficiency of the ASE process. The slopes are calculated and plotted in Fig. 5 for all prepared films. The quantum efficiency increases with increasing the film thickness indicating better

© The Institution of Engineering and Technology 2018

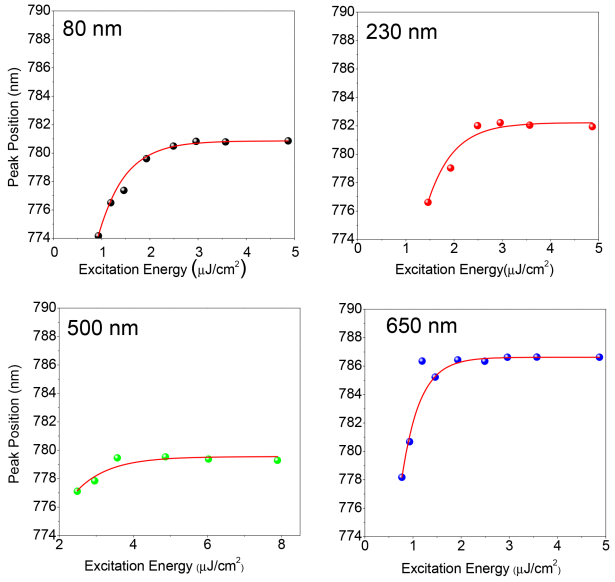

Fig. 3 *Peak position versus excitation energy for $MAPbI_3$ perovskite films of different thicknesses*

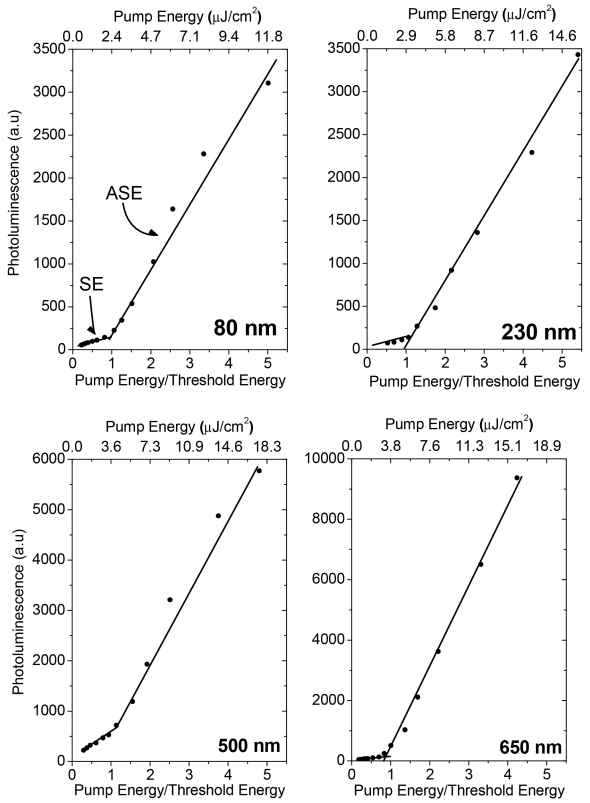

Fig. 4 *ASE pump energy thresholds of perovskite ($MAPbI_3$) films at different film thicknesses*

quality of the films prepared at higher thicknesses. This thickness dependent variation is further investigated by the calculations of the ASE threshold carrier density below.

3.2 Energy dependent carrier density calculations

From a fundamental point of view, the balance between absorption and stimulated emission rates gives rise to the optical gain. The lifetime of the excited state in perovskite films may last for ~10–100 ns [24, 28, 31], which gives higher opportunity to achieve higher rates of stimulated emission necessary for lasing. To accurately account for the film thickness and the thickness-dependent absorption, the excited carrier density has to be evaluated for each pump fluency. This way, the effect of film

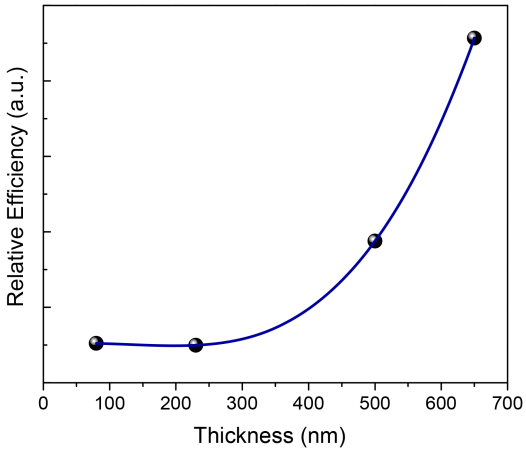

Fig. 5 *Slope (relative efficiency) versus film thickness for perovskite ($MAPbI_3$) films*

absorption on the resulting PL will be eliminated and the films can be directly compared for their optical activities [9].

Carrier density can be estimated from the absorbed photon density, which depends on the film thickness. The total number of photons n_{ph} in the pulse can be estimated using the following relation:

$$n_{ph} = \frac{E_{pulse}}{(hc/\lambda_{excitation})}, \quad (1)$$

where E_{pulse} is the energy of the incident laser pulse. The number of absorbed photons n_{abs} depends on the film thickness and absorption coefficient. Both film thickness and absorption coefficient are included in the absorbance that is presented in Fig. 1, where

$$n_{abs} = n_{ph} - n_{ph}\exp(-A), \quad (2)$$

where A is the absorbance ($A = \alpha\, d$) at the excitation wavelength, α is the absorption coefficient, and d is the film thickness. Assuming no losses, each absorbed photon will then result in one excited electron in the conduction band (carrier). In a unit volume, the number of excited electrons $n_{\text{excited electrons}}$ has to be divided by the excitation volume $\pi r^2 d$, where r is the beam radius and d is the film thickness in order to eventually estimate the charge carrier density (n).

Fig. 6 shows the PL versus carrier density curves for all samples. Noticeably, the relation between PL and carrier densities does not follow with the static relation trend in Fig. 4. When the film thickness is increased, the ASE threshold is anti-intuitively decreased until saturation is reached above 500 nm film thickness. The ASE threshold carrier density decreases from 7.73×10^{18} to 3.29×10^{18} cm^{-3} when the film thickness is increased from 80 to 650 nm.

This result can be explained by the existence of surface defects, which increases as the thickness decreases. At higher thickness, the percentage of surface defects to the whole film volume will be low, which is reflected by a higher quantum efficiency of the film as well. At 80 nm thickness, the higher surface/volume ratio results in a higher density of surface traps, which increase the ASE threshold carrier density. Additionally, the spin-coating deposition of perovskite films with homogeneous and complete coverage becomes more critical for thinner films, which results in other possible origins of surface defects (e.g. deposition of islands rather than compact films [32]). Surface defects will work as traps for excited carriers, which will prevent their recombination to produce ASE photons. When the film thickness is increased, the ASE threshold is subsequently decreased until saturation is reached at the 650 nm film, beyond which the ASE behaviour is mainly dominated by the bulk properties of the grown films. Fig. 7

© The Institution of Engineering and Technology 2018

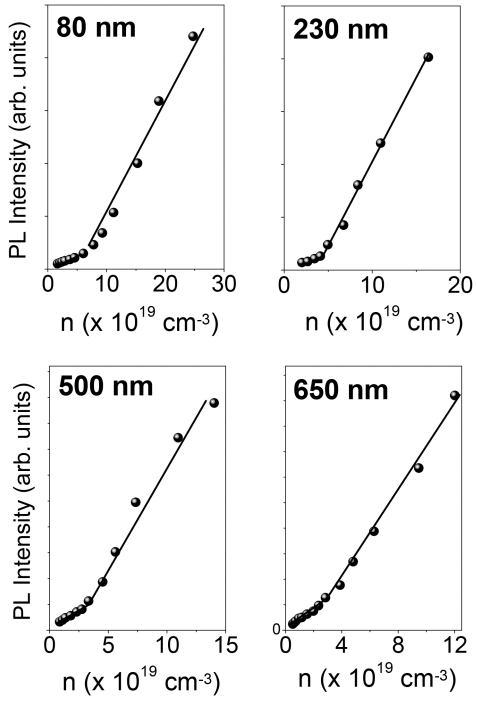

Fig. 6 *PL versus carrier density for $MAPbI_3$ perovskite films of different thicknesses*

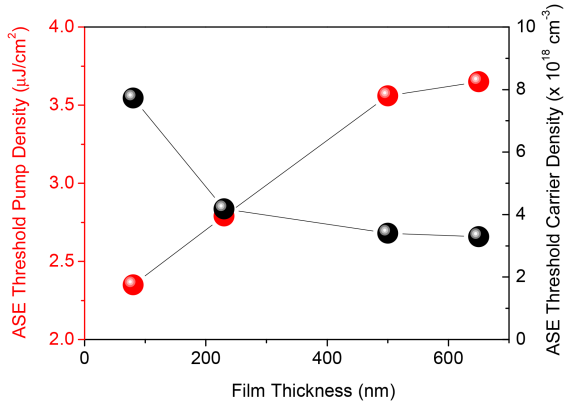

Fig. 7 *Dependence of both ASE threshold pump energy and ASE threshold carrier density of perovskite films with different film thicknesses*

compares the thickness dependence of both ASE threshold pump energy and ASE threshold carrier density.

3.3 Band gap renormalisation (BG) coefficient

BGR is also studied in this work and observed as a systematic red-shift of the ASE emission with increasing pump energy. BGR is a many-body problem of charge carriers in semiconductors, where interactions of electrons and holes under high population conditions ultimately result in narrowing the bandgap [33, 34]. BGR can be estimated using the following formula [32]:

$$\Delta E = 2\gamma n^{1/3}, \tag{3}$$

where ΔE is the renormalised value of the bandgap at high-carrier densities, γ is the bandgap renormalisation (BGR) coefficient, and n is the carrier density. The redshift in the emission peak with increasing pump power can be used to estimate BGR under respective pump powers. As mentioned above, the surface traps at small thicknesses result in reduced efficiency of radiative recombination, which result in higher ASE threshold carrier density and reduced quantum efficiency. Therefore, the 650 nm thick sample (at which ASE threshold carrier density saturates; see Fig. 7 and the discussion thereafter) is the closest sample that represent the intrinsic properties of bulk $MAPbI_3$ perovskite.

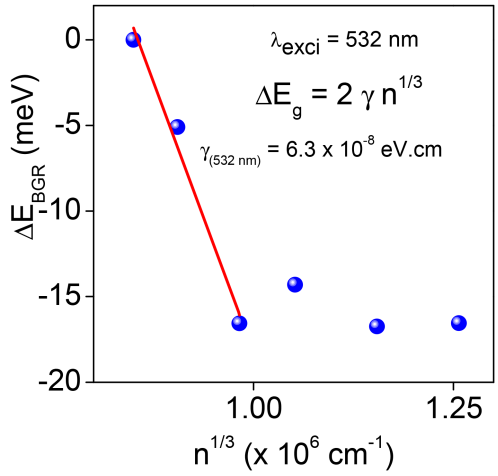

Fig. 8 *BGR versus $n^{1/3}$ of a perovskite film with 650 nm thickness under 532 nm excitation*

Accordingly, the BGR coefficient is evaluated for the 650 nm sample as can be seen in Fig. 8, which shows the plot of ΔE versus $n^{1/3}$ for the 650 nm particular sample. Due to the 3D and cavity-free structure of the present sample and the relatively big laser spot size of ~2 mm, different scattering and other gain losses can likely result in a gain clamping condition [35]. As a result of gain clamping, the carrier density does not increase significantly when increasing the fluence. Since saturation of gain at higher carrier densities prevent further renormalisation of the bandgap, only the first points above ASE threshold are used to extract the BGR coefficient. From the slope of the fitting line, the BGR coefficient could be estimated to be $\sim 6.3 \times 10^{-8}$ eV cm.

4 Conclusion

In conclusion, the effect of film thickness on the ASE behaviour of high-quality $CH_3NH_3PbI_3$ perovskite films is investigated and is shown to be an influential factor in their ASE behaviour. The film thickness turned out to have a determining role on the final optical properties of the perovskite films. The ASE threshold carrier density is doubled when the thickness is decreased from 650 to 80 nm, mostly attributed to the development of surface traps with small thicknesses. Further investigation of the traps involved, and subsequently improving the fabrication steps, should rather minimise this effect. BGR is observed in the prepared films as a redshift in the ASE peak with pump power, with a BGR coefficient of $\sim 6.3 \times 10^{-8}$ eV Cm.

5 Acknowledgments

This project was supported by King Saud University, Deanship of Scientific Research, College of Science Research Center.

6 References

[1] Burschka, J., Pellet, N., Moon, S.-J., *et al.*: 'Sequential deposition as a route to high-performance perovskite-sensitized solar cells', *Nature*, 2013, **499**, (7458), pp. 316–320

[2] Liu, M., Johnston, M.B., Snaith, H.J.: 'Efficient planar heterojunction perovskite solar cells by vapour deposition', *Nature*, 2013, **501**, (7467), pp. 395–398

[3] Tan, Z.-K., Moghaddam, R.S., Lai, M.L., *et al.*: 'Bright light-emitting diodes based on organometal halide perovskite', *Nat. Nanotechnol.*, 2014, **9**, (9), pp. 687–692

[4] Qaid, S.M.H., Al Sobaie, M.S., Majeed Khan, M.A., *et al.*: 'Band-gap tuning of lead halide perovskite using a single step spin-coating deposition process', *Mater. Lett.*, 2016, **164**, (135), pp. 498–501

[5] Sutherland, B.R., Sargent, E.H.: 'Perovskite photonic sources', *Nat. Photonics*, 2016, **10**, (5), pp. 295–302

[6] Zhu, K., Zhao, Y.: 'Organic–inorganic hybrid lead halide perovskites for optoelectronic and electronic applications', *Chem. Soc. Rev.*, 2016, **45**, (3), pp. 655–689

[7] Chen, S., Roh, K., Lee, J., *et al.*: 'A photonic crystal laser from solution based organo-lead iodide perovskite thin films', *ACS Nano*, 2016, **10**, (4), pp. 3959–3967

© The Institution of Engineering and Technology 2018

[8] Mitzi, D.B., Wang, S., Feild, C.A., *et al.*: 'Conducting layered organic-inorganic halides containing -oriented perovskite sheets', *Science*, 1995, **267**, (5203), pp. 1473–1476

[9] Arora, N., Dar, M.I., Hezam, M., *et al.*: 'Photovoltaic and amplified spontaneous emission studies of high-quality formamidinium lead bromide perovskite films', *Adv. Funct. Mater.*, 2016, **26**, (17), pp. 2846–2854

[10] Xing, G., Mathews, N., Lim, S.S., *et al.*: 'Low-temperature solution-processed wavelength-tunable perovskites for lasing', *Nat. Mater.*, 2014, **13**, (5), pp. 476–480

[11] Deschler, F., Price, M., Pathak, S., *et al.*: 'High photoluminescence efficiency and optically pumped lasing in solution-processed mixed halide perovskite semiconductors', *J. Phys. Chem. Lett.*, 2014, **5**, (8), pp. 1421–1426

[12] Dhanker, R., Brigeman, A.N., Larsen, A.V., *et al.*: 'Random lasing in organo-lead halide perovskite microcrystal networks', *Appl. Phys. Lett.*, 2014, **105**, (15), p. 151112

[13] Sutherland, B.R., Hoogland, S., Adachi, M.M., *et al.*: 'Conformal organohalide perovskites enable lasing on spherical resonators', *ACS Nano*, 2014, **8**, (10), pp. 10947–10952

[14] Zhu, H., Fu, Y., Meng, F., *et al.*: 'Lead halide perovskite nanowire lasers with low lasing thresholds and high quality factors', *Nat. Mater.*, 2015, **14**, (6), pp. 636–642

[15] Liao, Q., Hu, K., Zhang, H., *et al.*: 'Perovskite microdisk microlasers self-assembled from solution', *Adv. Mater.*, 2015, **27**, (22), pp. 3405–3410

[16] Zhang, Q., Ha, S.T., Liu, X., *et al.*: 'Room-temperature near-infrared high-Q perovskite whispering-gallery planar nanolasers', *Nano Lett.*, 2014, **14**, (10), pp. 5995–6001

[17] Wang, Y., Li, X., Song, J., *et al.*: 'All-inorganic colloidal perovskite quantum dots: a new class of lasing materials with favorable characteristics', *Adv. Mater.*, 2015, **27**, (44), pp. 7101–7108

[18] Yakunin, S., Protesescu, L., Krieg, F., *et al.*: 'Low-threshold amplified spontaneous emission and lasing from colloidal nanocrystals of caesium lead halide perovskites', *Nat. Commun.*, 2015, **6**, p. 8056

[19] Pan, J., Sarmah, S.P., Murali, B., *et al.*: 'Air-stable surface-passivated perovskite quantum dots for ultra-robust, single- and two-photon-induced amplified spontaneous emission', *J. Phys. Chem. Lett.*, 2015, **6**, (24), pp. 5027–5033

[20] Zhao, Y., Zhu, K.: 'CH_3NH_3Cl-assisted one-step solution growth of $CH_3NH_3PbI_3$: structure, charge-carrier dynamics, and photovoltaic properties of perovskite solar cells', *J. Phys. Chem. C*, 2014, **118**, (18), pp. 9412–9418

[21] Im, J.-H., Lee, C.-R., Lee, J.-W., *et al.*: '6.5% efficient perovskite quantum-dot-sensitized solar cell', *Nanoscale*, 2011, **3**, (10), p. 4088

[22] Chen, C.-C., Hong, Z., Li, G., *et al.*: 'One-step, low-temperature deposited perovskite solar cell utilizing small molecule additive', *J. Photonics Energy*, 2015, **5**, (1), p. 57405

[23] Jung, H.S., Park, N.: 'Perovskite solar cells: from materials to devices', *Small*, 2015, **11**, (1), pp. 10–25

[24] Li, Y., Yan, W., Li, Y., *et al.*: 'Direct observation of long electron-hole diffusion distance beyond 1 micrometer in $CH_3NH_3PbI_3$ perovskite thin film', *Sci. Rep.*, 2015, **5**, (1), p. 14485

[25] Stranks, S.D., Wood, S.M., Wojciechowski, K., *et al.*: 'Enhanced amplified spontaneous emission in perovskites using a flexible cholesteric liquid crystal reflector', *Nano Lett.*, 2015, **15**, (8), pp. 4935–4941

[26] Yang, D., Xie, C., Sun, J., *et al.*: 'Amplified spontaneous emission from organic-inorganic hybrid lead iodide perovskite single crystals under direct multiphoton excitation', *Adv. Opt. Mater.*, 2016, **4**, (7), pp. 1053–1059

[27] Stranks, S.D., Burlakov, V.M., Leijtens, T., *et al.*: 'Recombination kinetics in organic-inorganic perovskites: excitons, free charge, and subgap states', *Phys. Rev. Appl.*, 2014, **2**, (3), p. 34007

[28] D'Innocenzo, V., Grancini, G., Alcocer, M.J.P., *et al.*: 'Excitons versus free charges in organo-lead tri-halide perovskites', *Nat. Commun.*, 2014, **5**, (1), p. 3586

[29] Wehrenfennig, C., Liu, M., Snaith, H.J., *et al.*: 'Charge carrier recombination channels in the low-temperature phase of organic-inorganic lead halide perovskite thin films', *APL Mater.*, 2014, **2**, (8), p. 81513

[30] Priante, D., Dursun, I., Alias, M.S., *et al.*: 'The recombination mechanisms leading to amplified spontaneous emission at the true-green wavelength in $CH_3NH_3PbBr_3$ perovskites', *Appl. Phys. Lett.*, 2015, **106**, (8), pp. 1–5

[31] Zhang, Z.-Y., Wang, H.-Y., Zhang, Y.-X., *et al.*: 'The role of trap-assisted recombination in luminescent properties of organometal halide $CH_3NH_3PbBr_3$ perovskite films and quantum dots', *Sci. Rep.*, 2016, **6**, (1), p. 27286

[32] Yang, Y., Ostrowski, D.P., France, R.M., *et al.*: 'Observation of a hot-phonon bottleneck in lead-iodide perovskites', *Nat. Photonics*, 2015, **10**, (1), pp. 53–59

[33] Tränkle, G., Leier, H., Forchel, A., *et al.*: 'Dimensionality dependence of the band-gap renormalization in two- and three-dimensional electron-hole plasmas in GaAs', *Phys. Rev. Lett.*, 1987, **58**, (4), pp. 419–422

[34] Brinkman, W.F., Rice, T.M.: 'Electron-hole liquids in semiconductors', *Phys. Rev. B*, 1973, **7**, (4), pp. 1508–1523

[35] Bononi, A., Barbieri, L.: 'Design of gain-clamped doped-fiber amplifiers for optimal dynamic performance', *J. Lightwave Technol.*, 1999, **17**, (7), pp. 1229–1240

© The Institution of Engineering and Technology 2018